

3D Numerical modelling of faults for study of ground surface deformation using applied element method

Pradeep K. Ramancharla* and Kimiro Meguro

This article aims to understand the response of soil deposits underlying bedrock fault displacement in three dimensions. When an active bedrock fault ruptures, movement along the fault propagates through the overlying soil and produces zones of intense shear. Hence, it is important to study the surface behaviour based on fault characteristics. Hence we attempted to develop application of Applied Element Method by modelling the fault rupture zone. In this article, we have modelled the fault rupture problem in three dimensions. First, a simple model is used to illustrate absorption of the bedrock deformation by the overlying soil in elastic case. In the later part, nonlinear analysis is carried out to study the complex failure propagation in three dimensions. Influence of mechanical properties of the material is also discussed.

Keywords: Applied Element Method, ground surface deformation, strike-slip fault, surface rupture.

Two disastrous earthquakes occurred during the year 1999. The first one¹ was of magnitude 7.4 that occurred in Turkey on 17 August 1999. Immediately following that, another event² of magnitude 7.3 (Central Weather Bureau, Taiwan) occurred in Taiwan on 21 September 1999. The earthquake fault (North Anatolian Fault) in Turkey was traced over 100 km. The magnitude of right lateral movement of the fault on the ground surface was measured to be 2 to 4 m. In Taiwan, severe effects were observed. The earthquake fault (Cher-Lung-Pu Fault) was traced for about 80 km; here the fault movement directly caused severe damage. The magnitude of maximum vertical differential movement was measured to be nearly 10 m. The recent earthquake in Bhuj, India on 26 January 2001 also provided evidence of widespread liquefaction and ground deformation³. From the above two events it is clear that severe damage can be caused not only by strong ground motion but also by large surface deformations lying directly over the seismic faults. Hence, it is necessary to direct our efforts to study the relation between seismic fault characteristics, thickness of soil deposit and surface deformation.

Many researchers have conducted experiments to understand the phenomenon of surface failure. Cole and Lade⁴ have determined the location of surface fault rupture and width of the affected zone in alluvium over

dip-slip fault using fault test box. They hypothesized that the results may be applicable to cohesive materials. Lade *et al.*⁵ determined the multiple failure surfaces by conducting experiments on sand using fault test box. The results of the sand box model tests concluded that the observed displacement fields were largely the same for different materials. Onizuka *et al.*⁶ have modelled the deformation of ground using aluminum rods. Through experiments they investigated bedrock stresses induced by reverse dip-slip faults. Bray and coworkers⁷ investigated the pattern of ruptures in clay models under 1 g subjected to dip-slip faulting. The range of the dip angle of the bedrock varied from 60 to 90° for both normal and reverse faults. Tani *et al.*⁸ conducted a 1 g model study of dip-slip faulting using dry Toyoura sand as model material. Results from their first series of tests indicated that the base offset necessary for the rupture to propagate to the ground surface varied with fault orientation.

Using the above experimental methods, we can study the influence of length. However, replicating the actual field conditions using experiments is difficult, especially controlling the material properties and modelling the boundary conditions. Moreover, large amount of data are necessary to establish a relationship between seismic fault parameters and resulting surface deformation. On the other hand, studying this phenomenon using the numerical model has the advantage of controlling parameters like material properties, size of the model, boundary condition, dip angle, etc. Numerical models allow us to investigate a number of aspects of the fault rupture propagation phenomenon, which are difficult to study from examination of case histories or conduct of physical model tests.

Pradeep K. Ramancharla is in the Earthquake Engineering Research Centre, International Institute of Information Technology, Gachibowli, Hyderabad 500 019, India; Kimiro Meguro is in the Institute of Industrial Science, The University of Tokyo, 4-6-1 Komaba Meguro-Ku, Tokyo 153-8505, Japan.

*For correspondence. (e-mail: ramancharla@iiit.ac.in)

The discrete element approach intuitively looks promising. A soil mass is not a continuum. Instead, it is an assemblage of finite-sized particles. Inter-particle forces fundamentally determine the observed macroscopic behaviour of soil. Moreover, once a shear or tension crack develops within the soil mass, it becomes difficult to reliably apply a numerical approach based on the principles of continuum mechanics. The Extended Distinct Element Method⁹ however has a serious drawback in that it requires an enormous amount of calculation time, because explicit numerical integration is unstable unless the time step used is short⁹. A newly developed numerical model, the Applied Element Method (AEM)^{10–12} has many advantages over other discrete element methods. This method has been used to model fault motion in static¹³ and dynamic cases^{14,15}.

AEM

Here the extension of AEM to three dimensions is explained briefly. Two elements shown in Figure 1 are assumed to be connected by the sets of one normal and two shear springs. Each set represents the volume of elements connected. These springs totally represent stress and deformation of that volume of the studied elements. Six degrees of freedom are assumed for each element. These represent the rigid body motion of the element. Although the element motion is as a rigid body, its internal deformations are represented by spring deformation around each element. This means that the element shape does not change during

analysis, but the behaviour of element collection is deformable.

To have a general stiffness matrix, the location of the element and contact spring is assumed in a general position. The stiffness matrix components corresponding to each degree of freedom are determined assuming a unit displacement in the studied degree of freedom direction and by determining forces at the centroid of each element. The element stiffness matrix size is only 12×12 . Table 1 shows the components of the upper left quarter of the stiffness matrix. It is clear that the stiffness matrix depends on the contact spring stiffness and its location. The stiffness matrix given in Table 1 is for only one pair of contact springs. The global stiffness matrix is determined by summing up the stiffness matrices of individual pairs of springs around each element. Consequently, the developed stiffness matrix is an average stiffness matrix for the element according to the stress situation around the element. Using the advantage of the simplicity of AEM in formulation and accuracy in nonlinear range¹¹, fault rupture zone shown in Figure 2 is modelled.

Model preparation

There are three main types of faults, categorized according to the relative movement between the bedrock blocks, viz. strike-slip, dip-slip and thrust faults. In order to discuss the effect of strike-slip faults on the surface, we need to carry out the investigation using a 3D model. Hence, our attention is on the application of the numerical model 3D-

Table 1. One quarter of stiffness matrix

	(1)	(2)	(3)	(4)	(5)	(6)
(1)	$K_n N_x^2 + K_{1s} S_{1x}^2 + K_{2s} S_{2x}^2$	$N_x K_n N_y + S_{1x} K_{1s} S_{1y} + S_{2x} K_{2s} S_{2y}$	$N_x K_n N_z + S_{1x} K_{1s} S_{1z} + S_{2x} K_{2s} S_{2z}$	$K_n N_x (R_y N_z - R_z N_y) + K_{1s} S_{1x} (R_y S_{1z} - R_z S_{1y}) + K_{2s} S_{2x} (R_y S_{2z} - R_z S_{2y})$	$K_n N_x (R_z N_x - R_x N_z) + K_{1s} S_{1x} (R_z S_{1x} - R_x S_{1z}) + K_{2s} S_{2x} (R_z S_{2x} - R_x S_{2z})$	$K_n N_x (R_x N_y - R_y N_x) + K_{1s} S_{1x} (R_x S_{1y} - R_y S_{1x}) + K_{2s} S_{2x} (R_x S_{2y} - R_y S_{2x})$
(2)	$S(1, 2)$	$K_n N_y^2 + K_{1s} S_{1y}^2 + K_{2s} S_{2y}^2$	$N_y K_n N_z + S_{1y} K_{1s} S_{1z} + S_{2y} K_{2s} S_{2z}$	$K_n N_y (R_y N_z - R_z N_y) + K_{1s} S_{1y} (R_y S_{1z} - R_z S_{1y}) + K_{2s} S_{2y} (R_y S_{2z} - R_z S_{2y})$	$K_n N_y (R_z N_x - R_x N_z) + K_{1s} S_{1y} (R_z S_{1x} - R_x S_{1z}) + K_{2s} S_{2y} (R_z S_{2x} - R_x S_{2z})$	$K_n N_y (R_x N_y - R_y N_x) + K_{1s} S_{1y} (R_x S_{1y} - R_y S_{1x}) + K_{2s} S_{2y} (R_x S_{2y} - R_y S_{2x})$
(3)	$S(1, 3)$	$S(2, 3)$	$K_n N_z^2 + K_{1s} S_{1z}^2 + K_{2s} S_{2z}^2$	$K_n N_z (R_y N_z - R_z N_y) + K_{1s} S_{1z} (R_y S_{1z} - R_z S_{1y}) + K_{2s} S_{2z} (R_y S_{2z} - R_z S_{2y})$	$K_n N_z (R_z N_x - R_x N_z) + K_{1s} S_{1z} (R_z S_{1x} - R_x S_{1z}) + K_{2s} S_{2z} (R_z S_{2x} - R_x S_{2z})$	$K_n N_z (R_x N_y - R_y N_x) + K_{1s} S_{1z} (R_x S_{1y} - R_y S_{1x}) + K_{2s} S_{2z} (R_x S_{2y} - R_y S_{2x})$
(4)	$S(1, 4)$	$S(2, 4)$	$S(3, 4)$	$K_n (R_y N_z - R_z N_y)^2 + K_{1s} (R_y S_{1z} - R_z S_{1y})^2 + K_{2s} (R_y S_{2z} - R_z S_{2y})^2$	$K_n N_z (R_y N_z - R_z N_y) (R_z N_x - R_x N_z) + K_{1s} S_{1z} (R_y S_{1z} - R_z S_{1y}) (R_z S_{1x} - R_x S_{1z}) + K_{2s} S_{2z} (R_y S_{2z} - R_z S_{2y}) (R_z S_{2x} - R_x S_{2z})$	$K_n (R_y N_z - R_z N_y) (R_x N_y - R_y N_x) + K_{1s} (R_y S_{1z} - R_z S_{1y}) (R_x S_{1y} - R_y S_{1x}) + K_{2s} (R_y S_{2z} - R_z S_{2y}) (R_x S_{2y} - R_y S_{2x})$
(5)	$S(1, 5)$	$S(2, 5)$	$S(3, 5)$	$S(4, 5)$	$K_n (R_z N_x - R_x N_z)^2 + K_{1s} (R_z S_{1x} - R_x S_{1z})^2 + K_{2s} (R_z S_{2x} - R_x S_{2z})^2$	$K_n (R_z N_x - R_x N_z) (R_x N_y - R_y N_x) + K_{1s} (R_z S_{1x} - R_x S_{1z}) (R_x S_{1y} - R_y S_{1x}) + K_{2s} (R_z S_{2x} - R_x S_{2z}) (R_x S_{2y} - R_y S_{2x})$
(6)	$S(1, 6)$	$S(2, 6)$	$S(3, 6)$	$S(4, 6)$	$S(5, 6)$	$K_n (R_x N_y - R_y N_x)^2 + K_{1s} (R_x S_{1y} - R_y S_{1x})^2 + K_{2s} (R_x S_{2y} - R_y S_{2x})^2$

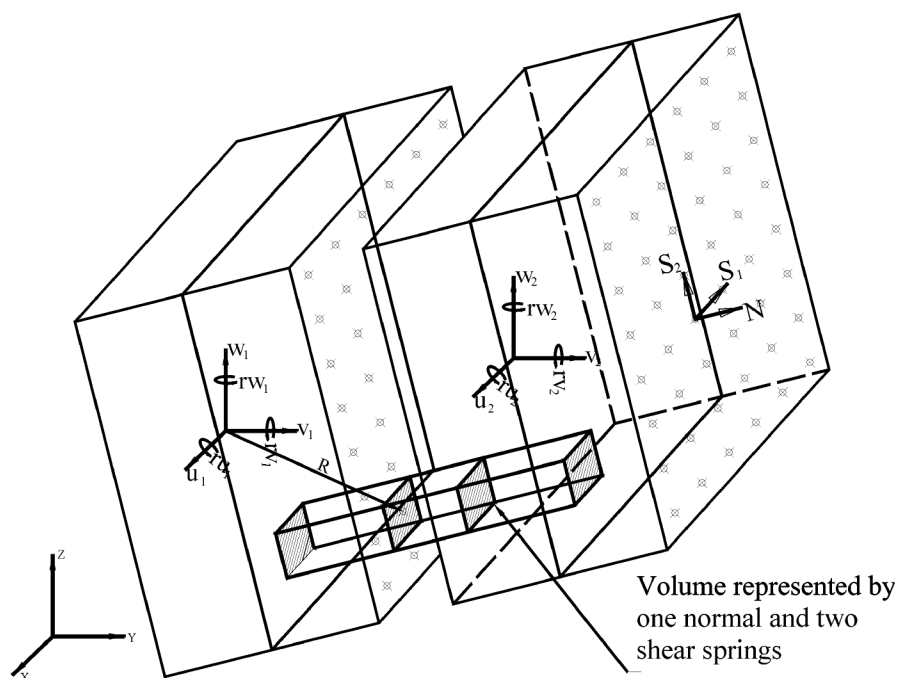


Figure 1. Element formulation in 3D AEM.

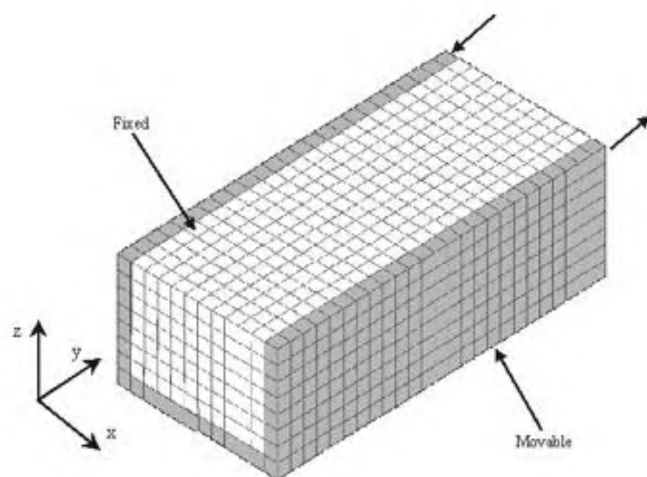


Figure 2. Numerical model for studying strike-slip fault.

AEM. Figure 2 shows the numerical model representing the left lateral strike-slip fault. This model is used to study the fault rupture propagation for strike-slip faults. The model is prepared using 2400 cube-shaped elements. Total size of the model is $120 \times 250 \times 80$ m and number of elements in each of the directions is $12 \times 25 \times 8$. The model size chosen here attempts the study of strike-slip fault with the 3D numerical method newly developed. The effect of element size is not considered while choosing the model size; however, the effect of thickness of the deposit is considered. The number of connecting springs on each face of the element is 25. Since this is the preliminary study, small size of the model is used.

Generally, soil strata and bedrock extend up to tens of kilometres in the horizontal direction. Numerical modelling of such a large medium is a difficult task. Moreover, to study the surface behaviour near the active fault region, it is necessary to model the small portion of the region that will include all the effects when the bedrock moves. To study the selected region numerically, we assumed the boundary on left side to be fixed. The bottom of the model is treated as bedrock, the left half is treated as fixed boundary and the right half as movable.

Linear modelling of faults

Analysis is carried out by giving the displacement equal to 5% (i.e. 3.5 m) of the thickness of the deposit. Initially, material of the deposit is considered as hard soil whose Young's modulus is taken as 2.5×10^5 kN/m². While conducting the parametric study, the effect of variation of elasticity of the deposit is considered. Figure 3 shows the deformation of the centre line at various depths in the deposit. From this figure, it can be seen that the deformation is absorbed inside the deposit. Originally the elements in a straight line attain different deformations at different heights. At the bottom of the deposit near the bedrock, the total offset is seen. However, when we move towards the ground surface, deformation becomes less. This is due to the elastic properties. The mechanical properties of the surficial materials sheared by the fault can significantly affect the surface deformation pattern. The inherent deformability of soils ensures that a fraction of the total offset

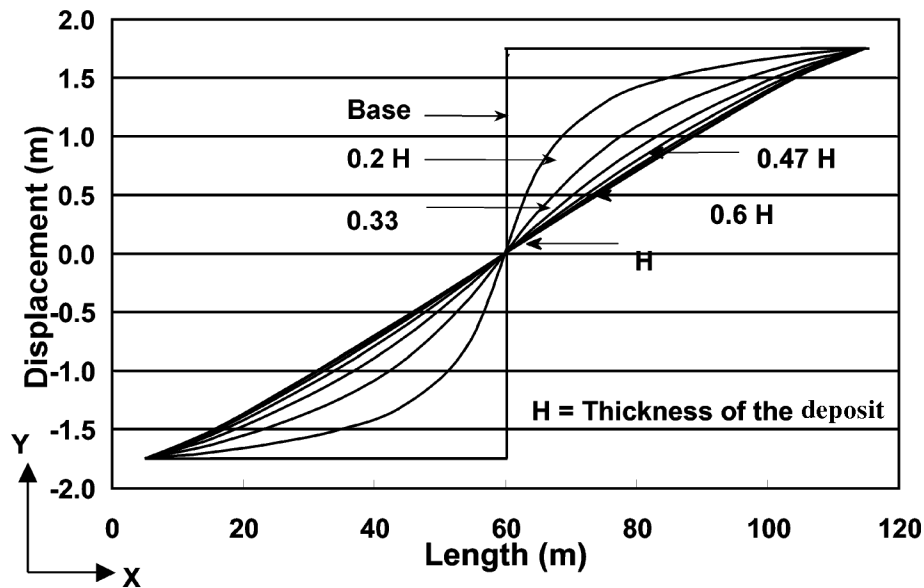


Figure 3. Centre line deformation at various depths in the deposit.

across a distinct base rock fault (occurring commonly in a narrow zone) will be distributed across a relatively larger mass of overlying deformed soil, and hence, the distinct offset at the ground surface will be typically less than that at the bedrock–soil contact. This effect depends on the properties of the material overlying the active fault. These observations may prove important in developing effective techniques to mitigate faulting-induced damage. For example, on the one hand, a ductile compacted fill placed over a potentially active bedrock fault will partly absorb the distinct base fault movement as deformation. Therefore, the surface differential movements and extensional strains in this zone will be smaller. However, the base fault offset will be distributed across a relatively wide area, possibly affecting numerous neighbouring structures. On the other hand, a stiffer, more brittle fill overlying the fault one will tend to concentrate that distinct base rock offset in a narrower area, and transfer more of the base offset to the ground surface.

Based on analyses of the resulting patterns of surface deformation after the 1906 San Francisco earthquake, Reid¹⁶ rendered an early and clear interpretation of the simultaneous occurrence of fractures and deformation in a deformable soil being sheared by an underlying bedrock strike-slip fault movement (Figure 4). Originally straight, horizontal lines at various depths in the deposit along line C–A attain different positions, i.e. C'–A', 1–1, 2–2, and 3–3, after the bedrock fault ruptures. The key observation Reid made was that the overlying soil could absorb part of the distinct base offset as deformation, thus generating a complex interaction of individual fractures and global shear deformation. Apparently, for more deformable, or equivalently, more ductile soil, larger base offsets can be absorbed before the ground surface ruptures.

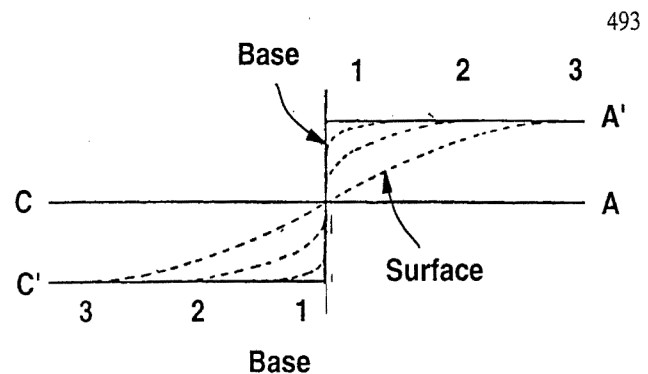


Figure 4. Interpretation of distribution in plan view of a distinct base offset propagating in overlying deformable deposit (Reid¹⁶).

Stresses and strain contours at different sections

Figure 5 shows horizontal deformation of the straight line adjacent to where the rupture is taking place. From Figure 5, it can be seen that the lines initially straight near the bedrock, and deforms in the horizontal direction perpendicular to the plane of rupture. This deformation increases as we move from the bedrock towards the ground surface. When we closely look at this phenomenon in three dimensions, we see that it produces Reidel shear pattern. In order to have a detailed understanding of this phenomenon, let us look at the displacement field inside the deposit. Figure 6 shows displacements at various levels (15, 45 and 75 m) normal (Figure 6 a) and parallel to the fault (Figure 6 b) directions respectively. From the displacement normal to the fault (Figure 6 a), it can be seen that at a height of 15 m from bedrock, the displacement is positive at one end and negative at the other end. This is due to the anti-

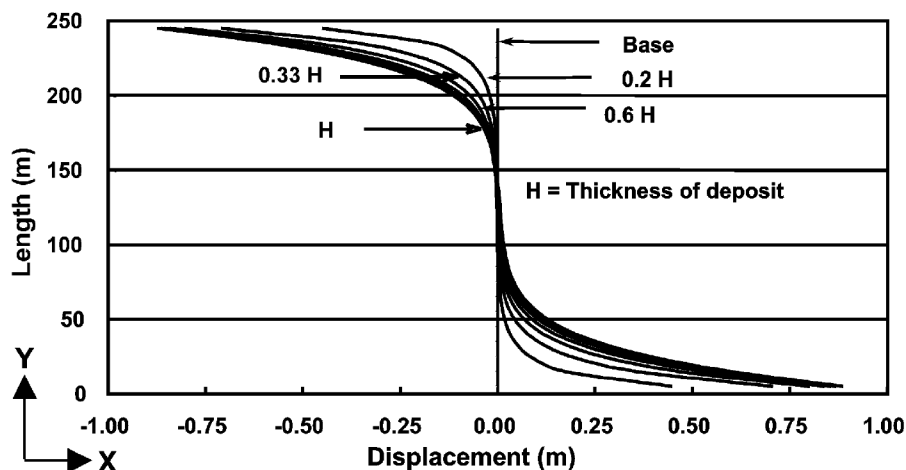


Figure 5. Deformation at various depths in the deposit.

clockwise moment produced by the movement of left lateral strike-slip fault. This lateral displacement normal to the fault increases when we move towards the surface at 45 and 75 m. While observing displacement parallel to the fault shown in Figure 6b, we can easily see that the deformation is uniform over the length of the fault in the close proximity of the bedrock. However, when we move towards the surface, this deformation reduces slightly at both the ends. The reason for this is the magnitude of shear stress that reduces near the surface at both the edges. From Figure 6b, it can be observed that the displacement parallel to the fault increases towards the boundary. The magnitude of this displacement is maximum near the bedrock and reduces towards the surface.

Nonlinear modelling of faults

Material properties adopted for nonlinear analysis are:

$E = 2.5 \times 10^5 \text{ kN/m}^2$; tensile strength, $\sigma_t = 1.5 \times 10^3 \text{ kN/m}^2$ and compressive strength, $\sigma_c = 1.5 \times 10^4 \text{ kN/m}^2$.

Pure strike-slip fault

The amount of base offset necessary for a strike-slip fault to propagate to the ground surface can be a critical factor when siting astride an active fault. This parameter, which depends on the mechanical properties of the surficial materials, also depends on the kinematic and geometric constraint of the problem. However, although kinematic and geometric effects play a major role in fault rupture propagation through the soil, they have not been adequately studied and quantified¹⁷. As with various problems in geotechnical engineering, rupture patterns can be significantly influenced by kinematic boundary conditions. Geometric effects also can be important. For instance, the amount of bedrock

offset necessary for the rupture to be expressed at the ground surface depends on the thickness and geometry of the soil deposit or earth structure being ruptured by the underlying fault. To advance our understanding of surface faulting, it is necessary to identify the controlling factors in the fault process. Among all the factors that affect the phenomenon characterizing surface rupture, the most important ones are: (i) the type of fault movement (normal, reverse, strike-slip), (ii) inclination of the fault plane, (iii) the amount of displacement on the fault, (iv) depth and geometry of the overlying earth materials, (v) characteristics of the overlying earth materials, and (vi) history of faulting, which includes fault age, slip-rate and the maximum offset per event.

An interesting observation provided by Naylor *et al.*¹⁸ was the three-dimensional reconstruction of individual shear ruptures. They noticed that because of the existing kinematic conditions (i.e. a concentrated fault at the base and the overall shear movement), adjacent en echelon *R* shears evolved from disconnected segments at the surface to a single rupture at the base. Therefore, it can be hypothesized that at the surface the orientation of the initial *R* shears was influenced by dilatancy and possibly strength of the sand; whereas near the base this orientation was solely governed by the existing kinematic boundary conditions.

Figure 7 shows the baseline deformation at various depths in the soil deposit. Figure 7 is similar to Figure 3 except for the case of nonlinearity of the material property. It can be seen from Figure 7 that the absorption of deformation inside the deposit is not uniform like in the elastic case. Here, cracks were generated when the stresses inside the material reached the material capacity. Figure 8 shows the propagation of cracks along the centre line. Each point in Figure 8 indicates the location of the failure spring, which in turn indicates the location where maximum shear takes place. It can be seen from Figure 8 that maximum shear takes place near the base rock and as we

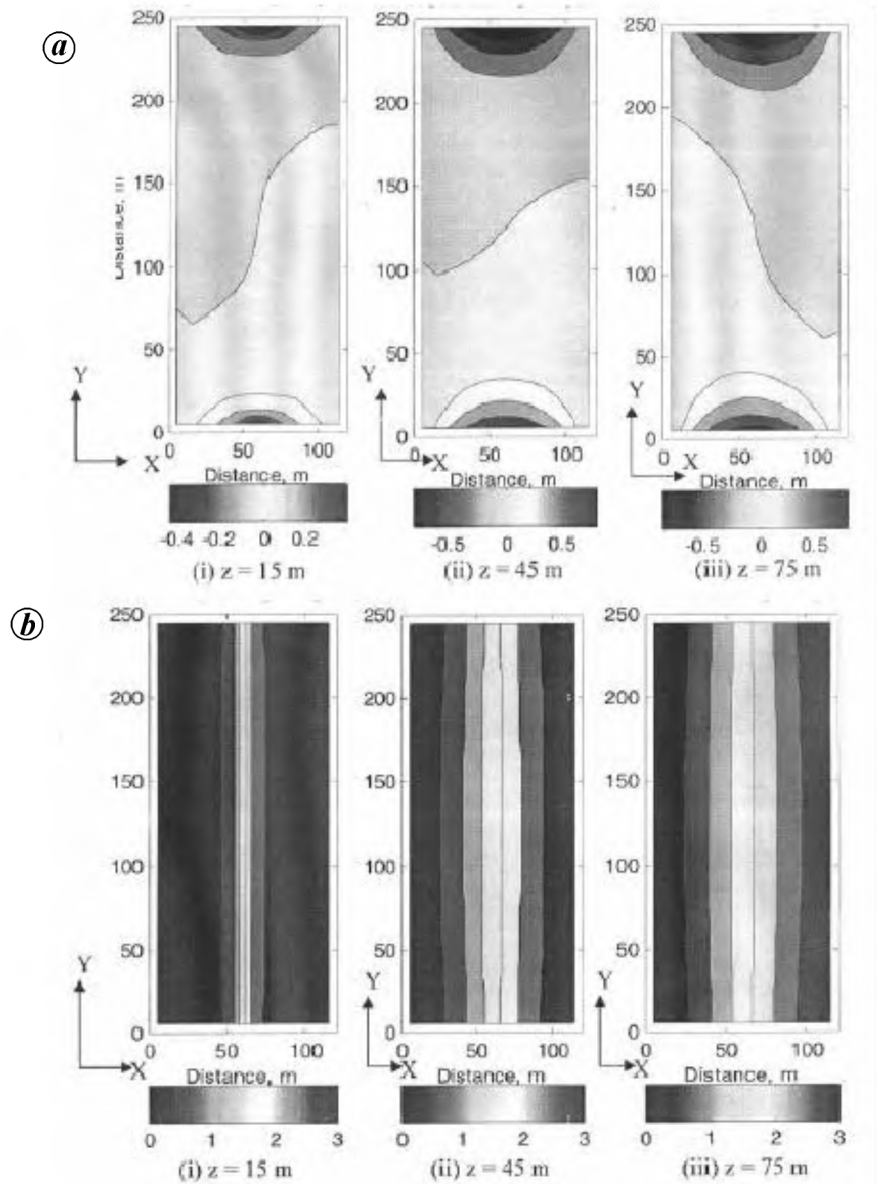


Figure 6. Deformation contours at various depths in the deposit. Displacement contour (a) normal and (b) parallel to the fault.

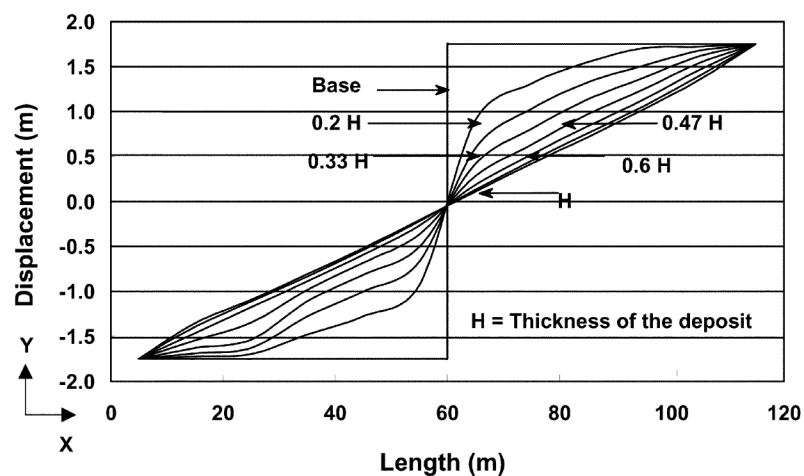


Figure 7. Baseline deformation at various depths using AEM.

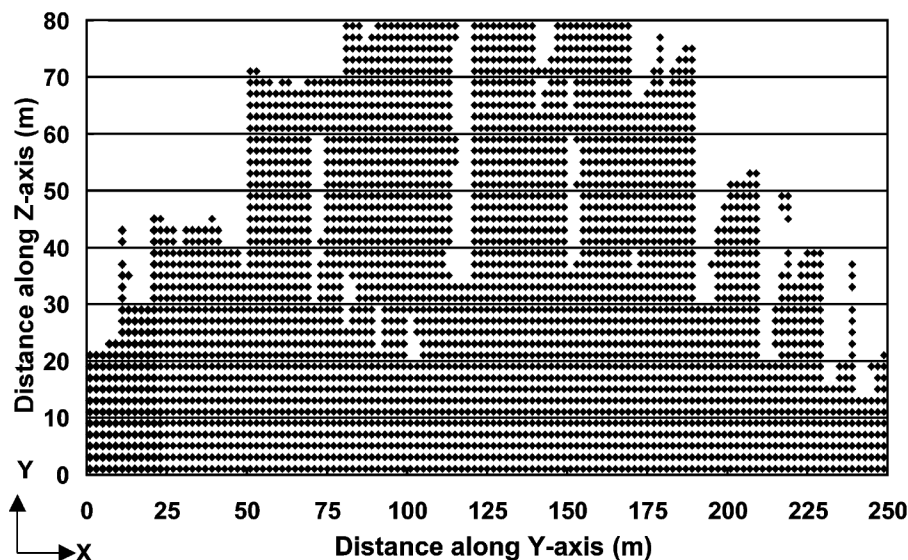


Figure 8. Propagation of cracks along centre line.

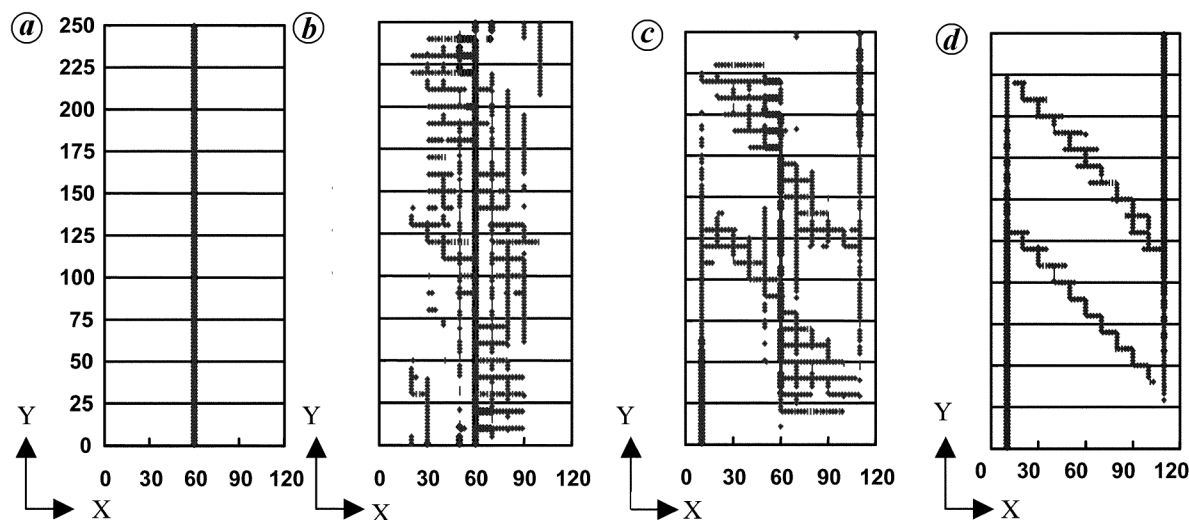


Figure 9. Evolution of cracks from bedrock to ground surface (a) $Z = 5$ m; (b) $Z = 25$ m; (c) $Z = 55$ m and (d) $Z = 75$ m.

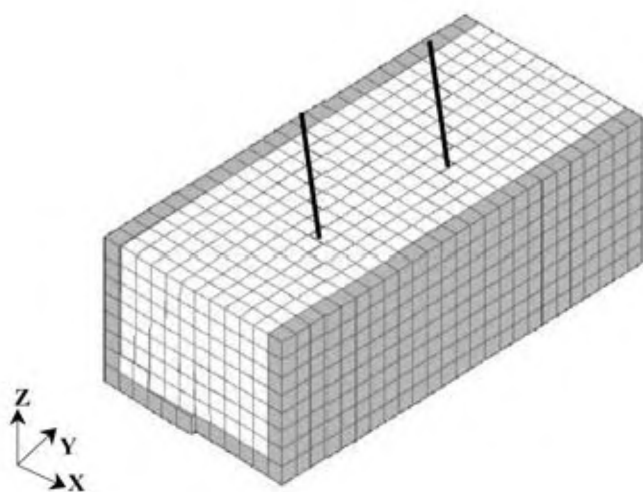


Figure 10. Element location and crack patterns.

move to the surface its influence is concentrated in the narrow zone. This effect can be understood when we look at the crack pattern observed on the ground surface (Figure 9). Figure 9 shows evolution of the cracks from the bedrock up to the surface. It can be clearly seen that the cracks that are distributed in the wider zone near the bedrock become concentrated in the smaller zone when they reach the surface. Figure 9 clearly indicates the evolution of an echelon pattern. And more clear view of crack distribution on the ground surface can be seen in Figure 10.

Effect of elastic material properties of soil deposit

Deformable capacity of the soil deposit is one of the important parameters on which the surface rupture depends. To check the effect of elastic material properties on the defor-

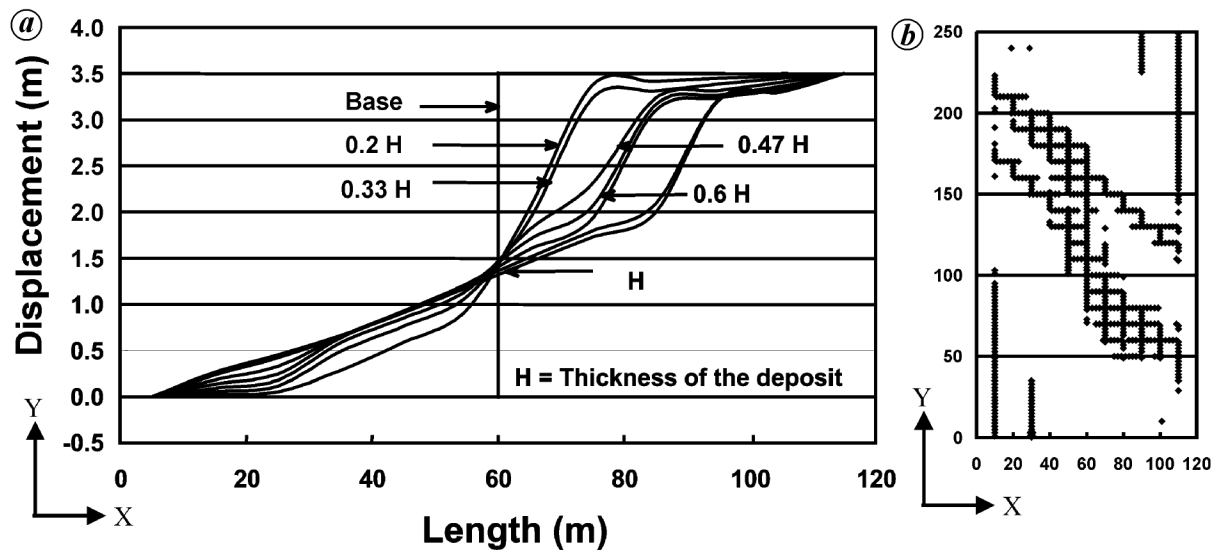


Figure 11. Effect of elastic material property (case 1, $\sigma_1 = 5.0 \times 10^3$ kN/m²). *a*, Baseline deformation at various depths; *b*, Cracks on ground surface.

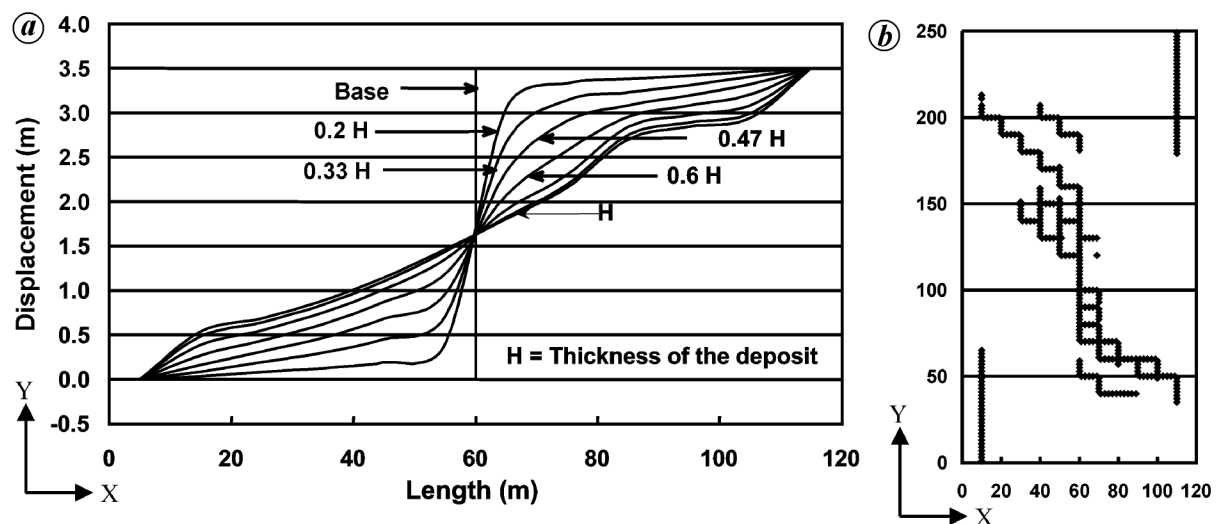


Figure 12. Effect of elastic material property (case 2, $E = 1.25 \times 10^5$ kN/m²). *a*, Baseline deformation at various depths; *b*, Cracks on ground surface.

mation of the deposit, two cases were studied by changing the stiffness of the deposit. Displacement of 5% of the thickness of the deposit is given to the movable block. First, the modulus of elasticity is increased, i.e. the analysis is carried out using relatively harder material, $E = 5 \times 10^5$ kN/m² (case 1). Figure 11 *a* shows the baseline deformation and Figure 11 *b* shows the crack pattern observed on the surface. From Figure 11 *a* it can be seen that the deformation of the baseline at various depths is not uniform like the deformation pattern for elastic case as shown in Figure 3. This is due to the brittleness of the material. From this, it is clear that harder material tend to transfer more base offset to the ground. This can be un-

derstood better if we observe Figure 11 *b*. Here the crack that is parallel to the fault near the bedrock rotates and intersects the centre line at nearly 45°. In this case there is only one major crack that intersects the baseline. Whereas in the earlier case (Figure 9) two cracks form the en echelon pattern. This means that if the material is softer, more deformation is absorbed inside the soil deposit and there is appearance of the en echelon pattern. To discuss this effect, analysis is carried out by reducing the material stiffness, i.e. $E = 1.25 \times 10^5$ kN/m² (case 2). Figure 12 *a* and *b* is similar to Figures 11 *a* and *b*. From these figures, it can be seen that due to the deformable capacity, more base offset is absorbed inside the deposit,

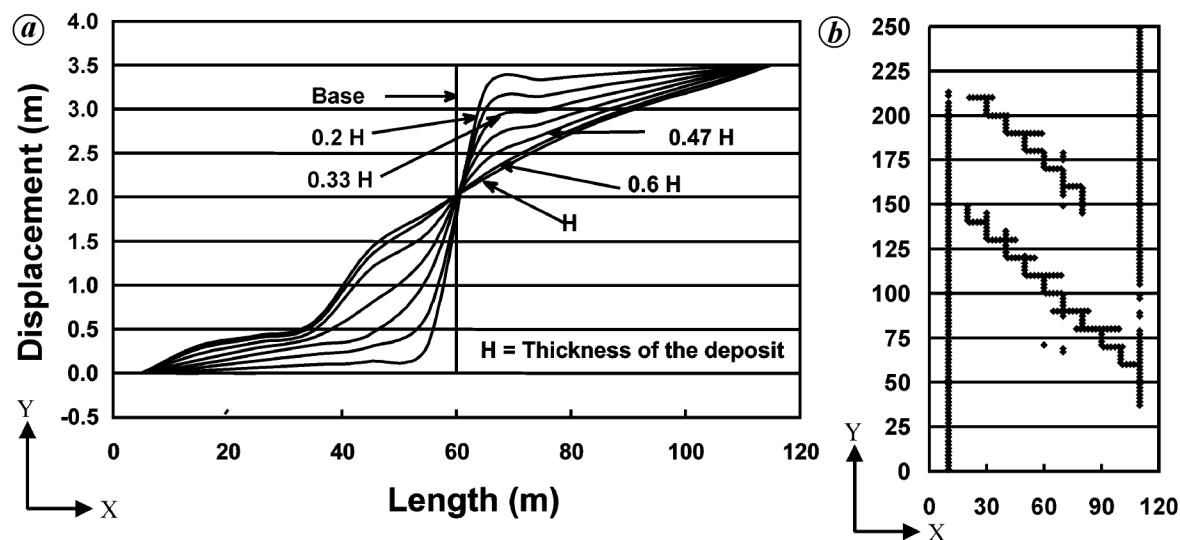


Figure 13. Effect of material strength (case 3, $\sigma_t = 3.0 \times 10^3 \text{ kN/m}^2$). *a*, Baseline deformation at various depths; *b*, Cracks on ground surface.

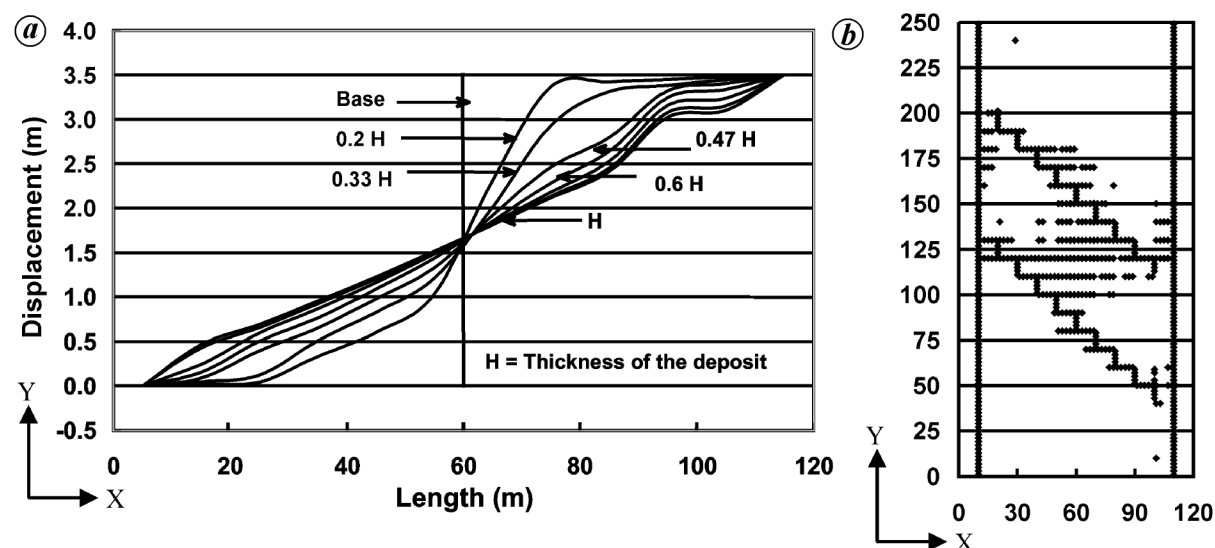


Figure 14. Effect of material strength (case 4, $\sigma_t = 0.75 \times 10^3 \text{ kN/m}^2$). *a*, Baseline deformation at various depths; *b*, Cracks on ground surface.

thus affecting the wide area on the surface. From Figures 13 *b* and 14 *b*, clear appearance of en echelon pattern on the surface can be seen.

Effect of material strength of soil deposit

Material strength is another important parameter on which the evolution of surface rupture from the seismic bedrock depends. To understand this, analysis is carried out first by increasing the material strength to double its value, i.e. $\sigma_t = 3.0 \times 10^3 \text{ kN/m}^2$ (case 3) and later by reducing the material strength to 50% i.e. $\sigma_t = 0.75 \times 10^3 \text{ kN/m}^2$ (case

4). In both these cases, stiffness is the same as in the case of Figure 7. Displacement of 5% of the thickness is given to the movable block and the effects are observed. Figure 13 *a* shows the baseline deformation and Figure 13 *b* shows the crack patterns observed on the surface. From Figure 13 *a*, it can be seen that the deformation of the baseline at various depths is not same as the deformation pattern for the elastic case, as shown in Figure 3. This is due to the change in material failure capacity. From this, it is clear that stronger materials tend to resist more base offset to the ground. However, for the prescribed displacement, the number of cracks that appear on the ground surface is less.

This can be understood better if we observe Figure 13 *b*. Here the crack that is parallel to the fault near the bedrock rotates and intersects the baseline at nearly 45° . In this case, the cracks are concentrated and intersect the baseline. Whereas in the earlier case, as shown in Figure 9, two cracks form the en echelon pattern. This means that if the material is stronger, less number of cracks appear on the surface. To discuss this effect, analysis is carried out by reducing the material strength. Figure 14 *a* and *b* is similar to Figure 11 *a* and *b*. From these figures, it can be easily seen that due to reduction in the material strength, more number of cracks appear on the surface, thus affecting a large area on the surface. From the above two cases, it can be said that the crack propagation velocity is inversely proportional to the strength of the material.

Effect of thickness of soil deposit

Thickness of the overlying soil deposit can be different in different places where the faults are buried. For similar movement of the buried fault, these deposits can produce different effects on surface deformation. Hence, analysis is carried out to find the influence of the thickness of the deposit on the distribution of cracks on the surface. First, thickness is increased (case 5), i.e. the model size is $120 \times 250 \times 90$ m and later thickness is reduced (case 6), i.e. the model size $120 \times 250 \times 60$ m is considered for analysis. Pure strike of 3.5 m is given to movable block. Figure 15 *a* and *b* shows baseline deformation at various depths and crack distribution on the ground surface respectively for case 5. From Figure 15 it can be seen that in the thicker

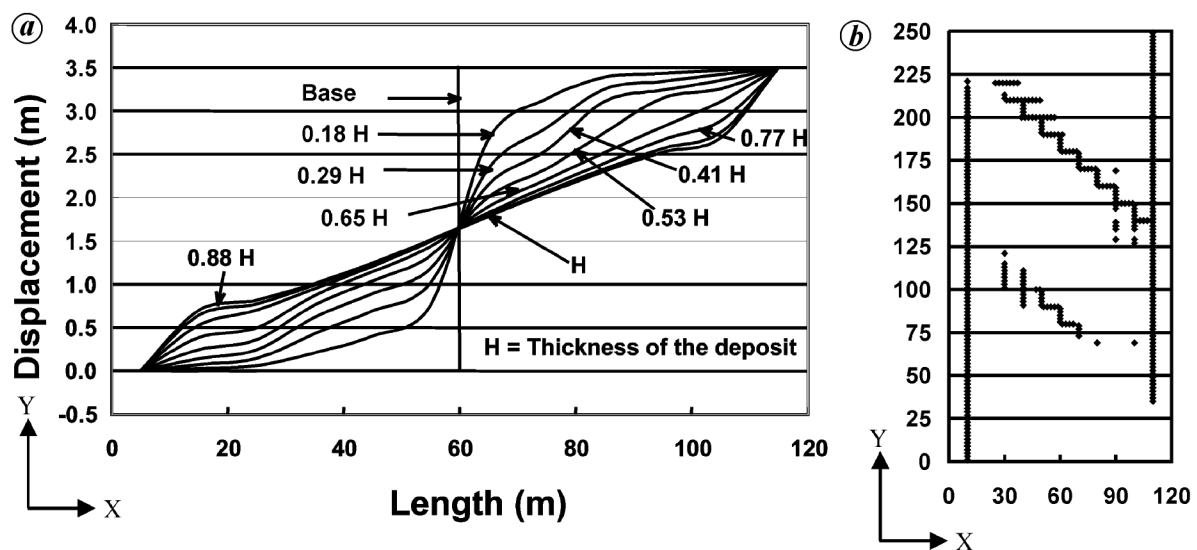


Figure 15. Effect of thickness (case 5, $H = 90$ m). *a*, Baseline deformation at various depths; *b*, Cracks on ground surface.

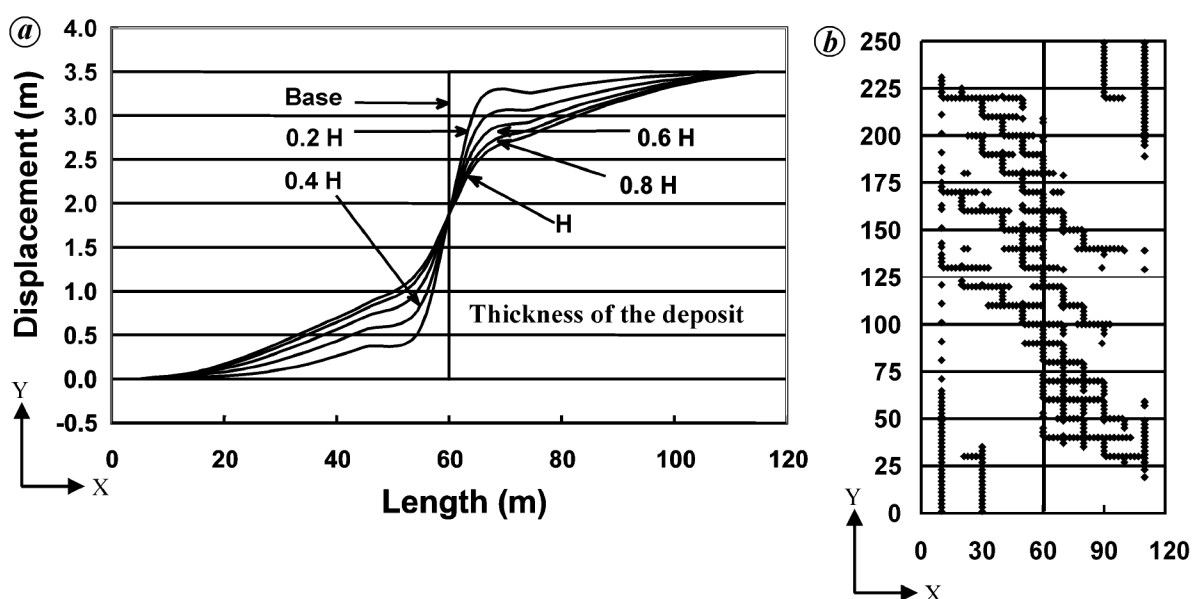


Figure 16. Effect of thickness (case 6, $H = 60$ m). *a*, Baseline deformation at various depths; *b*, Cracks on ground surface.

deposits, the number of cracks exposed on the surface is less. Figure 16 *a* and *b* shows baseline deformation at various depths and crack distribution on the ground surface respectively for case 6. From Figure 16, it can be seen that for the same amount of slip, faults that are buried at shallower depths can produce more cracks on the ground surface than those seated at greater depths.

Discussion and conclusion

Over the past few decades, significant efforts have been made to understand the problem of ground-shaking. Accordingly, numerous design and construction procedures have been developed to minimize damage due to strong ground motion. Such efforts towards the understanding the problem of surface faulting, however, have been relatively modest. The common practice with important facilities such as dams, nuclear power plants and public buildings has been to avoid construction across the recognized trace of an active fault. Still, avoidance is not always possible as certain project constraints may inevitably require a string of facilities across a fault. Furthermore, our ability to delineate all potential fault rupture zones and to assess their level of activity is far from complete. Therefore, techniques to minimize the damaging effects of surface faulting must be developed. Thus far, few techniques other than avoidance of construction near the recognized trace of a potentially active fault have been identified as effective strategies to mitigate the potential hazards associated with surface rupture. Hence, it is proposed here to study the response of soil deposits to underlying bedrock fault displacement. Particular attention will be given to strike-slip faulting.

When an active bedrock fault ruptures, movement along the fault propagates through the overlying soil and produces zones of intense shear. If the fault movement propagates up to or near the ground surface, damage to constructed facilities due to faulting, in conjunction with that induced by strong ground motion, can be significant. Moreover, the damage can be catastrophic if the fault propagates through a critical facility such as a dam. Although the effects of surface faulting occur in a significantly smaller area than where strong ground motion is felt, the hazard of surface faulting is also an important problem in geotechnical earthquake engineering because of the potentially adverse consequences of ground breakage.

On the contrary, from the recent earthquakes, it has been observed that structures which are located near the zone of faulting have survived and those that are far have experienced major damage. This shows that there is a strong relation between site conditions and the dynamic characteristics of wave motion. It is not easy to perform this investigation experimentally because it is difficult to prepare a model similar to the actual case. On the other hand, numerical models which can predict the behaviour of the medium

accurately in the small and large deformation range and in nonlinear range, have the advantage of modelling any kind of soil and possess the flexibility to change parameters such as strength of soil, thickness of deposit and dip angle. However, the main drawback in numerical modelling is to store huge amount of data of various parameters and large computation time. This drawback can be overcome with the use of high-speed computing facilities. In such a case, it is possible to discretize the numerical model into a mesh of finer sizes and store the time history of each parameter separately. Later, we can extract the stored data and perform necessary analyses to understand the influence of various parameters on ground deformation.

This kind of study is necessary to establish the possible locations of the faults appearing on the surface due to future earthquakes, because engineers are more concerned about the damage that might be caused when structures are located in vulnerable areas. From a seismological point of view, some difference between the real fault and the expected fault line is acceptable; but for engineers this difference sometimes might be a major concern.

An application to the 3D-AEM is developed here. Using a preliminary model, fault rupture propagation is studied in elastic and nonlinear cases. From the results, it can be concluded that the deformable soil deposit will partly absorb the distinct base offset. However, the base fault offset will be distributed across relatively wider area, possibly affecting numerous neighbouring structures. On the stiffer soil deposits, more cracks are exposed on the surface, whereas in the softer soil more deformation is absorbed inside the deposit resulting in lesser cracks on the surface. In the case of thinner overlying deposits, more cracks are exposed on the surface for same bedrock displacement compared to thicker deposits.

1. The 1999 Kocaeli earthquake, Turkey. Investigation into damage to civil engineering structures. Earthquake Engineering Committee, Japan Society of Civil Engineers, 1999.
2. The 1999 Ji-Ji earthquake, Taiwan. Investigation into damage to civil engineering structures. Earthquake Engineering Committee, Japan Society of Civil Engineers, 1999.
3. Rajendran, K., Rajendran, C. P., Thakkar, M. and Tuttle, M. P., The 2001 Kutch (Bhuj) earthquake: Coseismic surface features and their significance. *Curr. Sci.*, 2001, **80**, 1397–1405.
4. Cole Jr., D. A. and Lade, P. V., Influence zones in alluvium over dip-slip faults. *J. Geotech. Engg.*, 1984, **110**, 599–615.
5. Lade, P. V., Cole Jr., D. A. and David, D., Multiple failure surfaces over dip-slip faults. *J. Geotech. Engg.*, 1984, **110**, 616–627.
6. Onizuka, N., Hakuno, M., Iwashita, K. and Suzuki, T., Deformation in grounds and bedrock stress induced by reverse dip-slip faults. *J. Appl. Mech.*, 1999, **2**, 533–542.
7. Bray, J. D., The effects of tectonic movements on stresses and deformations in earth embankments. Ph D dissertation, University of California, Berkeley, 1990.
8. Tani, K., Ueta, K. and Onizuka, N., Scale effects of Quaternary ground deformation observed in model tests of vertical fault. In Proceedings 29th Japan National Conference of Soil Mecha-

- tics and Foundation Engineering, (in Japanese), 1994, pp. 1359–1562.
9. Hakuno, M. and Meguro, K., Simulation of concrete-frame collapse due to dynamic loading. *J. Eng. Mech.*, 1993, **119**.
 10. Meguro, K. and Tagel-Din, H., Applied element method for structural analysis: Theory and application for linear materials. *Struct. Eng./Earthq. Eng.*, 2000, **17**, 21s–35s.
 11. Meguro, K. and Tagel-Din, H., Applied element simulation of RC structures under cyclic loading. *J. Struct. Eng.*, 2001, **127**.
 12. Tagel-Din, H., A new efficient method for nonlinear, large deformation and collapse analysis of structures. Ph D thesis, Civil Eng. Dept., The University of Tokyo, 1998.
 13. Ramancharla, P. K. and Meguro, K., Nonlinear static modelling of dip-slip faults for studying ground surface deformation using applied element method. *Struct. Eng./Earthq. Eng.*, 2002, **9**, 169–178.
 14. Ramancharla, P. K. and Meguro, K., A study on the attenuation characteristics of peak responses in the near-fault region using applied element method. *Seisan Kenkyu*, 2001, **53**, 11–15.
 15. Ramancharla, P. K. and Meguro, K., Dynamic simulation of fault motion for studying ground surface deformation, In Proceedings 3rd International Summer Symposium, JSCE, August 2001, pp. 97–100.
 16. Reid, H. F., The mechanics of the earthquake in the California earthquake of 18 April 1906, Report, Carnegie Institute, Washington DC, 1910, vol. II.
 17. Lazarte, C. A., The response of earth structures to surface fault rupture, Ph D thesis, University of California, Berkeley, 1996.
 18. Naylor, M. A., Mandl, G. and Sijpesteijn, C. H. K., Fault geometries in basement-induced wrench faulting under different initial stress states. *J. Struct. Geol.*, 1986, **8**, 737–752.

Received 29 November 2004; revised accepted 19 June 2006